

Broken SU(6) symmetry and massive hybrid stars

Luiz L. Lopes¹

*Centro Federal de Educação Tecnológica de Minas Gerais Campus VIII; CEP 37.022-560,
Varginha - MG - Brasil*

Debora P. Menezes¹

*Universidade Federal de Santa Catarina; C.P. 476, CEP 88.040-900, Florianópolis, SC,
Brasil*

Abstract

In this work we revisit the quantum hadrodynamics (QHD) formalism to investigate hyperonic and hybrid stars with hyperon-meson couplings fixed via broken SU(6) group, in favor of a more general flavor group SU(3). We also employ an additional channel, the strangeness-hidden ϕ meson, which couples only to the hyperons. In hybrid stars, the quark phase is built with the SU(3) NJL model also with an additional vector channel in the Lagrangian. We found that within the models chosen the hyperon puzzle cannot be avoided by the quark-hadron phase transition, once the hyperon threshold always happens at lower density. Also, the contribution of the quark core in a hybrid star is more relevant to the radius than to the mass, and strongly depends on the quark equation of state. We are able to reproduce $2.21 M_{\odot}$ hyperonic star and $2.10 M_{\odot}$ hybrid star. Both results are in agreement with the recently detected hyper massive pulsar MSP J0740+6620.

Keywords: neutron stars, quark stars, hybrid stars, symmetry group

1. Introduction

Predicted by the Soviet physicist Lev Landau even before the discovery of the neutrons, neutron stars are the ultimate laboratory for cold strong inter-

Email address: llopes@cefetmg.br (Luiz L. Lopes)

acting matter, where the density in their cores can reach five to ten times the nuclear saturation density. The recent discovery of the hyper massive MSP J0740+6620, whose mass range lies at $2.14_{-0.09}^{+0.10} M_{\odot}$ with 68% credibility interval and $2.14_{-0.18}^{+0.20} M_{\odot}$ with 95% credibility interval [1], together with the well known PSR J0348+0432 with mass of $2.01 \pm 0.04 M_{\odot}$ [2], put strong constraints in the equation of state (EoS) of dense β -stable matter.

However, while the discovery of massive pulsars points to a very stiff equation of state (EoS), the onset of hyperons softens the very same EoS: as we increase the density towards the neutron star core, strange content particles - as hyperons - become energetically favorable, as the Fermi energy of the nucleons becomes of the order of their rest masses. The appearance of hyperons softens the EoS and reduces the possible maximum mass of the corresponding neutron star, which may cause a conflict between the astrophysical observations and the theoretical previsions. This is known as the hyperon puzzle. Although some studies indicate that the hyperon threshold can be suppressed by either very fast rotation [3] or by strong magnetic fields [4], this is not a consensus since a very similar formalism does not predict such suppression [5]. Nevertheless, these extreme conditions are not expected to be found in mostly observed pulsars. So, in these case, as was shown in an extensive study in ref. [6], hyperons - as Thanos - are inevitable [7].

Another possibility is that the observed pulsars are indeed quark stars, composed entirely by deconfined strange matter. If the Bodmer-Witten conjecture is true [9, 8], the protons and neutrons are not the true ground state of the strong interacting matter at high density, but rather the strange matter is the preferential ground state. If the density is high enough the star undergoes a phase transition from hadronic to strange matter causing all stellar matter to be converted into strange matter in a finite amount of time.

A different scenario happens if the strange matter is not the ground state, but yet is energetically favorable at high densities. In this case the core of the neutron star undergoes a phase transition to quark matter, while the outer layers are still formed by hadronic matter. A star with a quark core surrounded

by hadronic matter is called a hybrid star. A nice argument to corroborate this idea is based on the large N_c expansion as shown in ref.[10]. As the quark chemical potential exceeds the constituent quark mass, the increase of the pressure produces a phase where chiral symmetry is restored. With this hypothesis, for sufficiently high densities this matter becomes strange quark matter. A very recent study [11] suggests that the hybrid star is indeed the most probably scenario for massive neutron stars. According to this work, based on the sound velocity analyses, if stars are very massive $M \geq 2M_\odot$ a hybrid star scenario is favorable, while for stars around the canonical mass $M \simeq 1.4 - 1.5M_\odot$ a pure hadronic star is more probably.

To describe the hadronic matter we use the Quantum Hadrodynamics (QHD) formalism [12]. Here, besides the traditional σ , ω and ρ mesons [13], we employ the non-standard strangeness hidden ϕ meson [14, 15, 16, 17], which couples only to the hyperons. As pointed out in our previous work [18], the ϕ meson has a crucial role in the description of massive pulsars as the MSP J0740+6620. To fix the hyperon-meson coupling constants we break the hybrid SU(6) group in favor of a more general flavor SU(3) group, what allows us to fix all vector-meson coupling constants in terms of only one free parameter α_v .

In a previous work [15], we already studied how to use symmetry group to fix the hyperon meson coupling constants. Now we go beyond and also study quark matter in order to reproduce massive quark and hybrid stars. In the quark sector, we use the SU(3) Nambu Jona-Lasinio model NJL, which satisfies some QCD chiral symmetry aspects [19, 20]. As in the hadron phase, we employ an additional repulsive vector channel G_V , to stiff the EoS. Although G_V is treated as a free parameter, we impose some lattice QCD constraints to it [21]. Finally, hybrid star matter is obtained by imposing the Maxwell construction.

sectionHadronic neutron stars

Hadronic neutron stars - or simply neutron stars for short - are objects composed entirely by hadrons, as neutrons and protons. Additional degrees of freedoms as hyperons, Δ 's and boson condensates can also be present [13]. As the QCD, the natural tool of the standard model to describe strong interacting

matter produces no results for dense and cold matter, we have to employ effective models. Here we use the QHD, a relativistic model which describes the baryons as the fundamental degrees of freedom and describes their interactions via massive meson exchange.

To produce reliable neutron star properties we need to be able to reproduce realistic physical quantities that are known from phenomenology. There are five well known properties of symmetric nuclear matter at the saturation point: the saturation density itself (n_0), the effective nucleon mass (M^*/M), the compressibility (K), the symmetry energy (S_0) and the binding energy per baryon (B/A) [13]. Besides them, the symmetry energy slope (L) has attracted a lot of attention in the last years. Although its true value is still a matter of debate, most studies indicate that it has non-negligible implications on the neutron star macroscopic properties [22, 23, 24, 25, 27, 28, 29, 30]. To fulfill these constraints we use a slightly modified GM1 parametrization, which reduces the slope from 94 MeV to 87.9 MeV. This modification also causes a reduction in the symmetry energy from 32.5 MeV to 30.5 MeV and makes the parametrization closer to the acceptable ones according to the rigid constraints imposed in [26, 25].

The QHD Lagrangian in this work reads (Eq. (1)):

$$\begin{aligned} \mathcal{L}_{QHD} = & \sum_b \bar{\psi}_b \left[\gamma^\mu (i\partial_\mu - g_{b,\omega}\omega_\mu - g_{b,\rho}\frac{1}{2}\vec{\tau} \cdot \vec{\rho}_\mu) - (m_b - g_{b,\sigma}\sigma) \right] \psi_b + \frac{1}{2}m_\sigma^2\omega_\mu\omega^\mu \\ & + \frac{1}{2}m_\rho^2\vec{\rho}_\mu \cdot \vec{\rho}^\mu + \frac{1}{2}(\partial_\mu\sigma\partial^\mu\sigma - m_s^2\sigma^2) - U(\sigma) - \frac{1}{4}\Omega^{\mu\nu}\Omega_{\mu\nu} - \frac{1}{4}\mathbf{P}^{\mu\nu} \cdot \mathbf{P}_{\mu\nu}, \quad (1) \end{aligned}$$

in natural units. ψ_b are the baryonic Dirac fields. Here, not only nucleons can be present, but we also consider the possibility of the hyperon presence in the neutron star core. Because of the Pauli principle, as the number density increases, so does the Fermi energy. Ultimately the Fermi energy of the nucleons exceeds the mass of heavier baryons, and the conversion of some nucleons into hyperons [13] becomes energetically favorable. The σ , ω_μ and $\vec{\rho}_\mu$ are the mesonic fields. The g 's are the Yukawa coupling constants that simulate the strong interaction, m_b is the mass of the baryon b , m_s , m_v , and m_ρ are the masses of

the σ , ω , and ρ mesons respectively, The anti-symmetric mesonic field strength tensors are given by their usual expressions as presented in [13].

The $U(\sigma)$ is the self-interaction term introduced in ref. [31] to reproduce some of the saturation properties of the nuclear matter and is given by:

$$U(\sigma) = \frac{1}{3!}\kappa\sigma^3 + \frac{1}{4!}\lambda\sigma^4. \quad (2)$$

We also add the strangeness hidden ϕ meson, an additional vector channel that couples only to the hyperons [14, 16, 18]. Therefore it does not affect any of discussed nuclear saturation properties.

$$\mathcal{L} = g_{Y,\phi}\bar{\psi}_Y(\gamma^\mu\phi_\mu)\psi_Y + \frac{1}{2}m_\phi^2\phi_\mu\phi^\mu - \frac{1}{4}\Phi^{\mu\nu}\Phi_{\mu\nu}, \quad (3)$$

As neutron stars are stable macroscopic objects, we need to describe a neutral, chemically stable matter and hence, leptons are added as free Fermi gases:

$$\mathcal{L}_{lep} = \sum_l \bar{\psi}_l[i\gamma^\mu\partial_\mu - m_l]\psi_l, \quad (4)$$

where the sum runs over the two lightest leptons (e and μ).

In Tab. 1 we display the parameters of the slightly modified GM1 model as well as the prediction of the physical quantities and their inferred values from phenomenology [13, 32, 26, 25, 33].

As we allow the hyperon threshold, we also have to fix the hyperon-meson coupling constants. Unlike the nuclear matter, we have very little experimental information about hyperonic matter. The main term is the hyperon potential depth fixed at the saturation density. However, just the Λ hyperon has the potential depth well known at -28 MeV [32]. The knowledge of the other potential depths are known with a lower degree of precision, but widely accepted values are $U_\Sigma = +30$ MeV and $U_\Xi = -18$ MeV [22, 17]. Unfortunately the knowledge of the hyperon potential depth is not enough to fix all constants, once different sets of coupling constants reproduce the same potential values [34]. Even worst is the fact that these different sets of the coupling constants, yet predicting the same potential depth, cause large variations on the neutron star properties [13, 35]. So, in order to reduce the large number of free parameters, we

use symmetry group theory to fix the coupling of the hyperons with the vector mesons and the three potential depths to fix the coupling of the hyperons with the scalar meson.

In a previous work [18], we used the hybrid SU(6) group to fix all the vector mesons and a nearly SU(6) group to fix the scalar ones. Here, we relax this condition and break the SU(6) group in favor of the flavor SU(3) group [15, 17]. We impose that the Lagrangian is invariant and calculate the generalized SU(3) Clebsh-Gordon coefficients. We also consider an ideal mixing for the ω and ϕ mesons (A detailed study on hyperon-meson coupling constants within the context of symmetry groups can be found in our previous work. [15]. See also refs. [36, 37]). Within this approach, all the hyperon-meson coupling constants for the vector mesons become dependent of only one parameters, α_v .

	Parameters		Phenomenology	GM1	Masses (MeV)
$(g_{N\sigma}/m_s)^2$	11.785 fm^2	$n_0 \text{ (fm}^{-3}\text{)}$	0.148 - 0.170	0.153	$M_\Lambda = 1116$
$(g_{N\omega}/m_v)^2$	7.148 fm^2	M^*/M	0.7 - 0.8	0.7	$M_\Sigma = 1193$
$(g_{N\rho}/m_\rho)^2$	3.880 fm^2	$K \text{ (MeV)}$	220 - 315	300	$M_\Xi = 1318$
κ/M_N	0.005894	$S_0 \text{ (MeV)}$	30 - 35	30.5	$m_e = 0.511$
λ	-0.006426	$B/A \text{ (MeV)}$	15.7 - 16.5	16.3	$m_\mu = 105.6$
M_N	939 MeV	$L \text{ (MeV)}$	36 - 86.8	87.9	-

Table 1: **Modified** GM1 model parameters and physical quantities inferred from experiments [32, 26, 25, 33].

Therefore we have for the ω meson [15]:

$$\frac{g_{\Lambda\omega}}{g_{N\omega}} = \frac{4 + 2\alpha_v}{5 + 4\alpha_v}, \quad \frac{g_{\Sigma\omega}}{g_{N\omega}} = \frac{8 - 2\alpha_v}{5 + 4\alpha_v}, \quad \frac{g_{\Xi\omega}}{g_{N\omega}} = \frac{5 - 2\alpha_v}{5 + 4\alpha_v}. \quad (5)$$

For the ϕ meson we have:

$$\begin{aligned} \frac{g_{\Lambda\phi}}{g_{N\omega}} &= \sqrt{2} \left(\frac{2\alpha_v - 5}{5 + 4\alpha} \right), & \frac{g_{\Sigma\phi}}{g_{N\omega}} &= -\sqrt{2} \left(\frac{2\alpha_v + 1}{5 + 4\alpha_v} \right), \\ \frac{g_{\Xi\phi}}{g_{N\omega}} &= -\sqrt{2} \left(\frac{2\alpha_v + 4}{5 + 4\alpha_v} \right), & \frac{g_{N\phi}}{g_{N\omega}} &= 0. \end{aligned} \quad (6)$$

And finally for the ρ meson:

$$\frac{g_{\Sigma\rho}}{g_{N\rho}} = 2\alpha_v, \quad \frac{g_{\Xi\rho}}{g_{N\rho}} = 2\alpha_v - 1, \quad \frac{g_{\Lambda\rho}}{g_{N\rho}} = 0. \quad (7)$$

To solve the equations of motion, we use the mean field approximation (MFA), where the meson fields are replaced by their expectation values, i.e: $\sigma \rightarrow \langle\sigma\rangle = \sigma_0$, $\omega^\mu \rightarrow \delta_{0\mu} \langle\omega^\mu\rangle = \omega_0$, $\phi^\mu \rightarrow \delta_{0\mu} \langle\phi^\mu\rangle = \phi_0$ and $\rho^\mu \rightarrow \delta_{0\mu} \langle\rho^\mu\rangle = \rho_0$. Applying the Euler-Lagrange formalism to the sum of Eqs. (1) and (3) we obtain the following equation of motion:

$$[\gamma_0(i\partial^0 - g_{b,\omega}\omega_0 - g_{b,\phi}\phi_0 - g_{b,\rho}\rho_0) - i\gamma_j\partial^j - M_b^*]\psi_b = 0, \quad (8)$$

where we define $M_b^* \doteq m_b - g_{b,\sigma}\sigma_0$ as the effective baryon mass. Using the quantization rules ($E = i\partial^0$, $i\partial^j = k$) we easily obtain the eigenvalue for the energy:

$$E_b = \sqrt{k^2 + M_b^{*2}} + g_{b,\omega}\omega_0 + g_{b,\phi} + g_{b,\rho}\frac{I_{3b}}{2}\rho_0, \quad (9)$$

where I_{3b} is the isospin projector, and assumes the value of +1 for p, Σ^+ and Ξ^0 , zero for Λ^0 and Σ^0 and -1 for n, Σ^- , and Ξ^- .

When we set $\alpha_v = 1$, we recover the SU(6) parametrization for the vector mesons. In this case, the ω meson couples to hypercharge, while the ρ meson couples to isospin, as proposed by Sakurai [38].

Leptons are added as a free Fermi gas, with energy:

$$E_l = \sqrt{k^2 + m_l^2}. \quad (10)$$

To construct the equation of state (EoS) for this many body system of leptons and strongly interacting baryons we use the Fermi-Dirac statistics. As the thermal energy of a stable neutron star is much lower than the Fermi energy of its particles, $T = 0$ is a good approximation. For the baryons the solution for the energy density is straightforward [39]:

$$\epsilon = \frac{1}{\pi^2} \int_0^{k_f} \sqrt{k^2 + M_b^*} k^2 dk, \quad (11)$$

the same expression is valid for the leptons, we just have to replace the effective baryon mass M_b^* to the lepton mass m_l .

In MFA the contribution of the mesonic fields to the energy density is given by [13, 40, 15]

$$\epsilon_m = \frac{1}{2} \left(m_s^2 \sigma_0^2 + m_v^2 \omega_0^2 + m_\rho^2 \rho_0^2 \right) + U(\sigma), \quad (12)$$

The total energy density is the sum of the energy density of all fields (baryons, leptons and mesons). Finally the expected values of the mesonic fields are calculated either from the Euler-Lagrange equations or by imposing that the total energy density be stationary at fixed baryon density [13]:

$$\left(\frac{\partial \epsilon}{\partial \sigma_0} \right) = \left(\frac{\partial \epsilon}{\partial \omega_0} \right) = \left(\frac{\partial \epsilon}{\partial \rho_0} \right) = \left(\frac{\partial \epsilon}{\partial \phi_0} \right) = 0. \quad (13)$$

To calculate every particle population at a fixed density we impose electric charge neutrality and chemical equilibrium:

$$\mu_{bi} = \mu_n - e_{bi} \mu_e, \mu_\mu = \mu_e; \quad \sum_f e_f n_f = 0, \quad (14)$$

where μ_{bi} and e_{bi} are the chemical potential and electric charge of the i -th baryon respectively. At zero temperature, the chemical potentials coincide with the energy eigenvalues given in Eqs. (9) and (10); μ_e and μ_μ are the electron and muon chemical potential respectively; n is the number density and the sum in f runs over all the fermions.

To obtain the complete EoS we calculate the pressure via thermodynamics:

$$p = \sum_f \mu_f n_f - \epsilon, \quad (15)$$

1.1. Results

We next choose some values to α_v and calculate the vector meson coupling constants. In our previous work [15], we also fixed the scalar meson within symmetry group context. However, although the symmetry groups reproduce good results for α_v close to 1.0, as we move away from this value, the hyperon potential depths become unrealistic. So, here the scalar meson coupling constants are

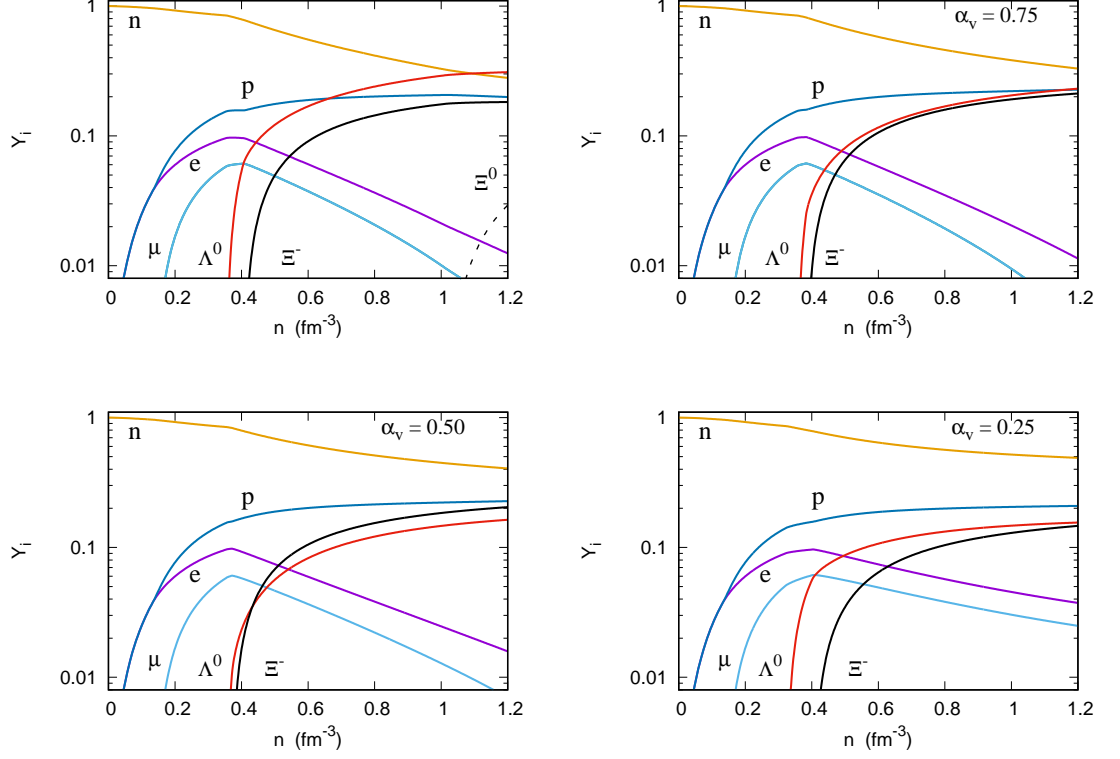


Figure 1: (Color online) Particle population for the SU(6) group and different values of α_v .

fixed in order to reproduce the more acceptable values of the potential depth: $U_\Lambda = -28$ MeV, $U_\Sigma = +30$ MeV and $U_\Xi = -18$ MeV. The calculated coupling constants are displayed in Tab. 2.

We plot in Fig. (1) the particle population for different values of α_v . We see that the hyperon population depends strongly on the hyperon-meson coupling constants. As we move away from the SU(6) ($\alpha_v = 1$) towards $\alpha_v = 0.25$, we see a suppression of the strangeness content particles. Indeed, only when $\alpha_v = 1$ we have the presence of Ξ^0 hyperon and only in this case, a strangeness content particle is the most populated particle - the Λ^0 - at very high densities ($n > 1 \text{ fm}^{-3}$). For $\alpha_v = 0.75$ the Λ^0 and the Ξ^- population are of the same order as the proton one. Reducing the value of α_v makes the neutron and the proton

-	$\alpha_v = 1.00$	$\alpha_v = 0.75$	$\alpha_v = 0.50$	$\alpha_v = 0.25$
$g_{\Lambda\omega}/g_{N\omega}$	0.667	0.687	0.714	0.75
$g_{\Sigma\omega}/g_{N\omega}$	0.667	0.812	1.00	1.25
$g_{\Xi\omega}/g_{N\omega}$	0.333	0.437	0.571	0.75
$g_{\Lambda\phi}/g_{N\omega}$	-0.471	-0.619	-0.808	-1.06
$g_{\Sigma\phi}/g_{N\omega}$	-0.471	-0.441	-0.404	-0.354
$g_{\Xi\phi}/g_{N\omega}$	-0.943	-0.972	-1.01	-1.06
$g_{\Sigma\rho}/g_{N\rho}$	2.0	1.5	1.0	0.5
$g_{\Xi\rho}/g_{N\rho}$	1.0	0.5	0.0	-0.5
$g_{\Lambda\sigma}/g_{N\sigma}$	0.610	0.626	0.653	0.729
$g_{\Sigma\sigma}/g_{N\sigma}$	0.403	0.514	0.658	0.850
$g_{\Xi\sigma}/g_{N\sigma}$	0.318	0.398	0.500	0.638

Table 2: Hyperon-meson coupling constants for different values of α_v . When we impose $\alpha_v = 1$ we recover the hybrid group SU(6).

the most populated particles for all densities. The suppression of the Ξ^- makes the lepton fraction to increase for low values of α_v . For instance, the muon population at 1 fm^{-3} is about 30 times higher in $\alpha_v = 0.25$ as compared with the SU(6) case. A curious case is $\alpha_v = 0.50$, being the only one which produces the Ξ^- instead of the Λ^0 as the most populated hyperon at high densities.

A more clever way to understand the suppression of strangeness content particle is, instead of looking at the individual hyperon population, look at the strangeness fraction, f_s , defined as:

$$f_s = \frac{1}{3} \frac{n_i |s_i|}{n}, \quad (16)$$

where s_i is the strangeness of the i -th baryon. The results are plotted in Fig. 2.

As we can see, there is a direct relation between α_v and the strangeness fraction, as also pointed in ref. [15]. When we move away from SU(6) we increase the repulsion of the hyperons, by increasing the $Y - \omega$ and the $Y - \phi$ coupling constants as shown in Tab. 2. This reduces the hyperon population at high

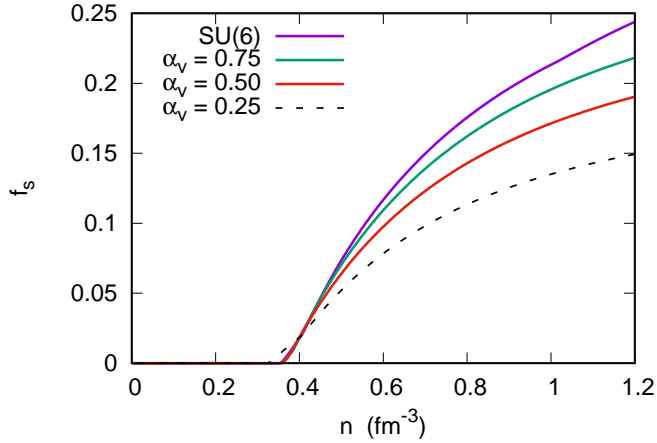


Figure 2: (Color online) Strangeness fraction as a function of α_v .

densities, reducing the strangeness fraction.

In Fig. 3 we plot the EoS and the respective mass-radius relation by solving the TOV equations [41] for the discussed values of α_v . As expected, there is a clear relation between the α_v and the maximum mass neutron star. As we reduce the value of α_v , we increase the value of ω and ϕ fields, increasing the hyperon repulsion. This makes the EoS stiffer, which in turn increases the maximum mass. As the EoS needs to be constrained by the massive known pulsars [2, 1], we use the MSP J0740+6620 mass range of $2.14^{+0.10}_{-0.09} M_\odot$ at 68% credibility interval (light blue) and $2.14^{+0.20}_{-0.18} M_\odot$ at 95% credibility interval (light yellow) as error bars. As we can see all parametrizations used in this work agree with the 95% credibility interval, while just the SU(6) lies out of the range of the 68% credibility interval. Our study indicates that massive neutron stars with hyperons are not ruled out. The main neutron star properties are shown in Tab. 3.

The maximum obtained mass varies from $2.00M_\odot$ for $\alpha_v = 1$ to $2.21M_\odot$ for $\alpha_v = 0.25$. We see that while the strangeness fraction drops from 20% to 12.9% for the maximum mass, the central density n_c hardly changes. Another important point concerns the radii of the canonical $1.4M_\odot$ stars. Although some

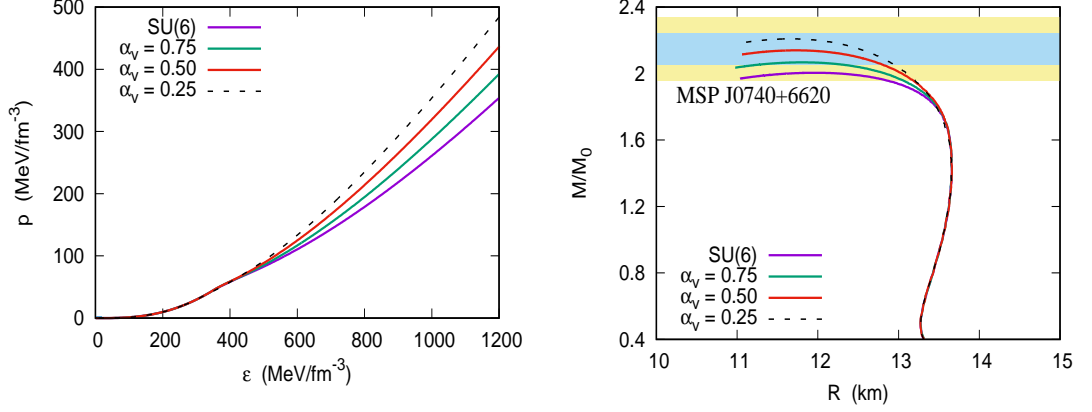


Figure 3: (Color online) (right) EoS and (left) mass-radius relation for a neutron star for different values of α_v . The hatched areas correspond to 68% and 95% credibility interval for the MSP J0740+6620.

α_v	M_{max}/M_{\odot}	$R(km)$	$n_c (fm^{-3})$	f_{sc}
SU(6)	2.00	11.95	0.92	0.200
$\alpha_v = 0.75$	2.07	11.80	0.93	0.185
$\alpha_v = 0.50$	2.14	11.73	0.94	0.164
$\alpha_v = 0.25$	2.21	11.67	0.93	0.129

Table 3: Neutron stars main properties for different values of α_v ; the subscript c means central density.

studies pointed out that the radii of the canonical stars could be as larger as 17 km [42], nowadays this value is believed to be significant lower. Conservative results point towards a maximum radius of 13.9 km [43], yet, more radical studies point to 13 km as the maximum radius [44, 27]. Studying the deformability parameter of the canonical star, the LIGO and Virgo collaboration stated that its value lies in the range $70 \leq \Lambda_{1.4} \leq 580$ [45] and this restriction imposed another constraint to the radius of the corresponding star. According to [46], the values should lie in the region $11.82 \text{ km} \leq R_{1.4M_{\odot}} \leq 13.72 \text{ km}$ and according to [45], in the range $10.5 \text{ km} \leq R_{1.4M_{\odot}} \leq 13.4 \text{ km}$. As for all our parametrizations

we have 13.68 km for $1.4M_{\odot}$ star (and no hyperon at such mass value), whichever constraint we consider correct, we see that our results for the radii are very close to the border of these ranges. Nevertheless, a very new result indicates that the canonical neutron star radius cannot exceed 11.9 km [47]. This radius value together with the mass of the MSP J0740+6620 may indicate that a profound revision either on the nuclear theory or the general relativity [48] may be needed. For instance, in ref. [49], we have shown that the onset of a new, yet unknown free parameter, can produce massive and compact neutron star families. However, this is not a closed subject, once recent results coming from NICER experiments [50, 51] as well neutron skins [52] point towards maximum radius values of 13.85 km, 14.26 km and 13.76 km respectively. We reinforce here that our result of 13.68 km agrees with ref. [50, 51, 52] besides ref. [43, 46].

2. Quark stars

In nature, deconfined quark matter certainly existed in the early universe when the temperature was very high. Up today, it is not clear if deconfined quark matter exists in the core of massive neutron stars. Moreover, if the Bodmer-Witten conjecture is true [9, 8], pulsars with central densities above a certain limit should be converted into strange stars. The main difference between quark stars - or strange stars - and the conventional neutron stars composed of baryons, is the fact that while the neutron star is bounded by gravity, strange stars are bounded by the strong force itself.

To describe a quark star, we need a quark matter EoS. As in the hadronic case, the natural tool to describe these matter is the QCD. And as we did before, we resort to an effective model. In the limit of vanishing quark masses, we expect the QCD to present chiral symmetry. Long before the QCD was known to be the theory of strong interactions, phenomenological indications for the existence of chiral symmetry came from the study of the nuclear β decay. An effective model that is well known to present these features is the Nambu Jona-Lasinio model [19]. Here we use its SU(3) version, whose Lagrangian includes a scalar,

a pseudo-scalar and the t'Hooft six-fermion interaction - needed to model the axial symmetry breaking [54, 55, 53] and reads:

$$\mathcal{L}_{NJL} = \bar{\psi}_f[\gamma^\mu(i\partial_\mu - m_f)]\psi_f + G_s \sum_{a=0}^8 [(\bar{\psi}\lambda_a\psi)^2 + (\bar{\psi}\gamma_5\lambda_a\psi)^2] - K\{det[\bar{\psi}(1 + \gamma_5)\psi] + det[\bar{\psi}(1 - \gamma_5)\psi]\} \quad (17)$$

where ψ_f are the quark Dirac fields, with three flavors, $m_f = \text{diag}(m_u, m_d, m_s)$ are the current quark masses, λ_a are the eight Gell-Mann flavor matrices and G_s and K are dimensionful coupling constants. Unlike the QHD model for baryons, where the interaction is mediated by massive mesons, the NJL model has no mediator, and the interaction is a direct quark-quark point-like scheme (see ref. [55] to see the Feynman diagrams). This makes the NJL a non-renormalizable model, and a cutoff is needed to obtain physical results. The SU(3) NJL is adjusted according to five main physical parameters: the π , η and σ meson masses, as well as the pion and η decay coupling constants, f_π and f_η . The parameters we choose to use (HK), the physical predictions and experimental values are given in Tab. 4.

	Parameters		Phenomenology	SU(3) NLJ
$m_u = m_d$	5.5 MeV	m_π (MeV)	128 -138	138
m_s	135.7 MeV	m_η (MeV)	487	549
Λ	631.4 MeV	m_σ (MeV)	668	700
$G_s\Lambda^2$	1.835	f_π (MeV)	93	93
$K\Lambda^5$	9.29	f_η (MeV)	94.3	84 - 102

Table 4: SU(3) NJL parameters and physical quantities inferred from experiments [55].

Now, as in the hadronic case, we add an additional vector channel. Here we use an universal vector coupling:

$$\mathcal{L}_{NJLv} = -G_V(\bar{\psi}\gamma^\mu\psi)^2. \quad (18)$$

In the phase diagram, the vector term weakens and delays the phase transition of the chiral restoration, and can potentially alter the nature from chiral transition to the color-superconducting (CSC) phase [56]. The mathematical formalism of the vector term shows that it acts similarly to the ω meson in QHD models, creating an additional repulsion between the quarks and stiffens the EoS [57]. This effect is desirable once we need to construct an EoS stiff enough to simulate the two solar mass MSP J074+6620 pulsar.

Assuming the mean field approximation (MFA) we can rewrite the quark-quark interaction in terms of the scalar condensates and the quark number density: [58]

$$\begin{aligned}(\bar{\psi}\psi)^2 &= 2\langle\bar{\psi}\psi\rangle\langle\bar{\psi}\psi\rangle - \langle\bar{\psi}\psi\rangle^2, \\ (\bar{\psi}\gamma^0\psi)^2 &= 2\langle\bar{\psi}\gamma^0\psi\rangle\langle\bar{\psi}\gamma^0\psi\rangle - \langle\bar{\psi}\gamma^0\psi\rangle^2.\end{aligned}\tag{19}$$

The dressed quark masses, M_f are determined by a coupled set of gap equations [53], where ϕ_f is the scalar quark condensed of flavor f : $\phi_f = \langle\bar{\psi}_f\psi_f\rangle$:

$$M_f = m_f - 4G_s\phi_f + 2K\phi_i\phi_j\tag{20}$$

with $i \neq j \neq f$ and:

$$\phi_f = \frac{-\nu M_f}{2\pi^2} \int_{k_{Ff}}^{\Lambda} \frac{k^2 dk}{\sqrt{M_f^2 + k^2}},\tag{21}$$

where k_{Ff} is the Fermi momentum of the quark f and $\nu = 6$ is the color-spin degeneracy factor. In the same way, the vector channel induces a displacement of the energy eigenvalue (as well as in the chemical potential at $T = 0$), i.e.,

$$E_f = \mu_f = \sqrt{M_f^2 + k_{Ff}^2} + 2G_V n,\tag{22}$$

where n is the total quark number density: $n = \sum_f n_f$. Now the energy density is obtained by taking into account the vacuum and the in-medium contributions. We can write [53, 59]

$$\epsilon = \sum_f \left[\frac{\nu}{2\pi^2} \int_{k_{Ff}}^{\Lambda} \sqrt{M_f^2 + k^2} k^2 dk + 2G_s \phi_f^2 \right] + G_V n^2 + 4K \phi_i \phi_j \phi_k - \epsilon_{vac},$$

where the constant ϵ_{vac} is the vacuum energy, introduced in order to set the energy density of the physical vacuum ($k_F = 0$) equal to zero. It is also worth mentioning that Eq. (18) is not the only way to introduce a vector channel in the NJL models (see ref. [53] for more details).

As in the hadronic case, leptons are added as a free Fermi gas, as required by charge neutrality and chemical stability. The relations between the chemical potentials and the number density of different particles are given by [60]:

$$\begin{aligned} \mu_s = \mu_d = \mu_u + \mu_e, \quad \text{and} \quad \mu_e = \mu_\mu, \\ n_s + n_\mu = \frac{1}{3}(2n_u - n_d - n_s). \end{aligned} \quad (23)$$

The energy density is obtained via the thermodynamic relation given in (Eq. 15).

In order to obtain physical results we need to fix the G_v coupling constant. While in QHD the non standard vector channel ϕ introduces no new free parameters because all hyperon-vector mesons can be fixed throughout symmetry group arguments, unfortunately, in the NJL, this is not the case. In most works the G_v is treated just as a free parameter [53, 58, 61, 59, 62]. Nevertheless, in other works, the authors have tried to fix the G_v coupling from direct comparisons with the lattice QCD (LQCD) results.

In ref. [56] studying the interplay between chiral transition and CSC phase, the authors fixed G_V in the range $0.2G_s < G_v < 0.3G_s$ in order to reproduce the LQCD; in ref. [63] G_v was fixed in the range $0.283G_s < G_v < 0.373G_s$ in order to reproduce the slope of the pseudo-critical temperature for the chiral phase transition at low chemical potential extracted from LQCD simulations; also to reproduce the pseudo-critical temperature, in ref. [64] G_V was found to be in the range $0.25G_s < G_V < 0.4G_s$ and finally, in ref. [21] a very restrictive

choice was made and the $G_V = 0.33G_s$. We use this value, $G_V = 0.33G_s$ as a limit of acceptable values that agree with the LQCD. We use then four different parametrizations for G_V : $G_V = 0.00$, $G_V = 0.11G_s$, $G_V = 0.22G_s$, and $G_V = 0.33G_s$. However, as the value $G_V = 1.0G_s$ up today can be found in the literature [53, 61, 59], we also use this value for matter of completeness and comparison. Nevertheless we have to keep in mind that such value is away above what is expected from LQCD.

2.1. Results

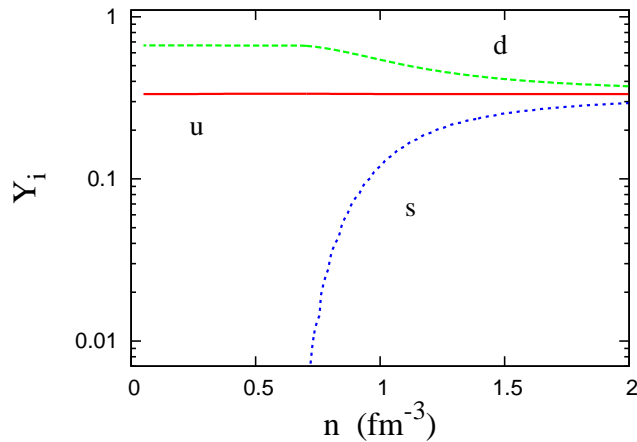


Figure 4: (Color online) The quark population for all values of G_V . Unlike in hadronic phase, the lepton population is insignificant for all densities.

In Fig. 4 we plot the particle population for all values of G_V . Unlike the baryon population, the quark population does not depend on the coupling constant because, as shown in Eq. (22), the displacement in the chemical potential is the same for all quarks and for all values of G_V . As G_s and K coupling constants are equal to all quarks, the main difference is generated by the mass of the s quark. With our choice following ref. [54], the s quark onset happens around 0.66 fm^{-3} . Also, the lepton population is insignificant through out the star. The electron population has a maximum of only $Y_e = 0.002$ next to the s

quark threshold, then it drops for higher densities. The muons are absent due to the fact that their mass is bigger than the mass of the light quarks.

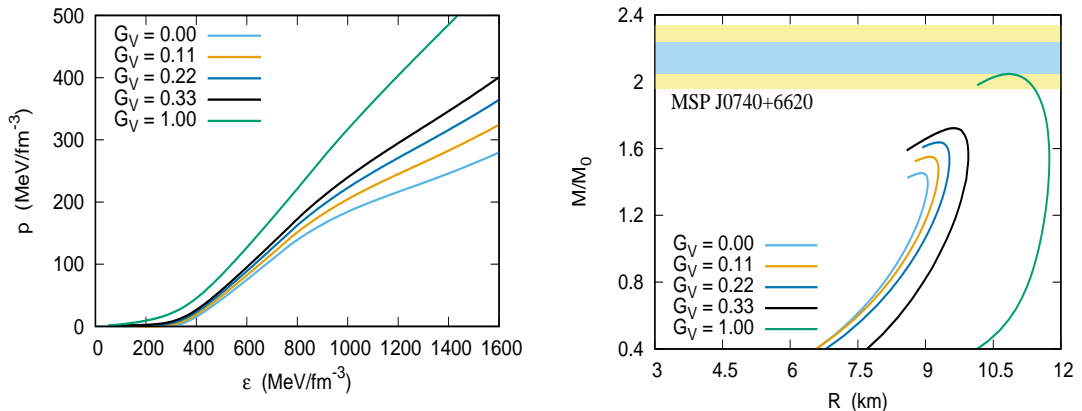


Figure 5: (Color online) (right) EoS and (left) mass-radius relation for a quark star for different values of G_V . Strength is the vector coupling, stiff is the EoS, as well higher is the maximum mass.

As for the EoS itself, it is plotted in Fig. 5 alongside some of the corresponding macroscopic properties of the quark stars, i.e., the mass-radius relation for the different values of G_V . As expected, there is a simple relation between the strength of the G_V and the EoS, which reflects in the maximum mass. Increasing the G_V , we stiff the EoS and increase the maximum mass. For realistic values of G_V , our maximum mass is quite below the experimental limit of the MSP J0740+6620. But, if we increase the value of G_V we are able to reproduce a 2.05 M_\odot quark star. Nevertheless we have to keep in mind that $G_V = 1.0G_s$ is way above the values expected from LQCD [21]. Therefore, instead of considering artificial and unphysical values of G_V , we accept the fact that massive neutron stars can hardly be described as quark stars. The main results are resumed in Tab. 5.

For realistic values of G_V , the maximum quark star masses varies from 1.46 M_\odot to 1.73 M_\odot . We also see that the higher the G_V value, the higher the radius of the maximum mass quark star. In general, quark stars are denser

G_V	M/M_\odot	$R(km)$	$n_c (fm^{-3})$	f_{sc}
$0.00G_s$	1.46	8.92	1.17	0.186
$0.11G_s$	1.55	9.12	1.16	0.184
$0.22G_s$	1.64	9.31	1.14	0.177
$0.33G_s$	1.73	9.59	1.10	0.165
$1.00G_s$	2.05	10.90	0.87	0.055

Table 5: Quark star main properties for different values of G_V .

than hadronic ones. On the other hand, increasing G_V causes a reduction of the central baryon number n_c . In the same way, it causes a reduction of the strangeness fraction. For $G_V = 1.00G_s$ the strangeness fraction is only 5.5%. Such low value is below the strangeness fraction found in hadronic stars, even with a strong hyperon-hyperon repulsion.

Also pointed out in ref. [61] and other references therein, the hadronic neutron star could be a meta-stable system, which eventually collapses. If the original neutron star had a mass beyond $1.73 M_\odot$ (the higher mass value for a realistic vector channel) it would become a black hole. However, a lower mass neutron star could become a quark star. The other possibility is that the metastable hadronic star can face a transition to a hybrid star [65], an object with both, hadron and quark matter [66], as discussed in the next section.

3. Hybrid Stars

As we said earlier, it is not clear if deconfined quarks are present in the core of massive pulsars. However, from a phenomenological point of the view, as the density increases towards the star core, quarks can become more energetically favorable than baryons, and ultimately the neutron star core may be composed of deconfined quarks. If the entire star does not convert itself into a quark star as suggested by the Bodmer-Witten conjecture, the final composition is a quark core surrounded by a hadronic layer. This is what is generally called a hybrid

star. Nevertheless the physics and formalism used to construct a hybrid star still present some bias.

Some authors [67, 68] suggest that the Maxwell construction is more suitable to build a hybrid star. Within Maxwell constructions the quark-hadron phase transition happens at constant pressure. However, it implies that the quark and the hadron phases are spatially separated and there is a discontinuity in the electron chemical potential, although the neutron chemical potential is continuous.

On the other hand ref. [13] argues that the Gibbs condition is better as Maxwell construction can be β unstable at the interface between the phases. In Gibbs condition the pressure and all chemical potentials (including the electron chemical potential) are continuous. Under these construction, instead of spatially separated phases, quarks and hadrons coexist in a mixed state, generating one intermediate phase in between the hadronic and the quark phases.

The differences between Maxwell and Gibbs construction was already checked in ref. [69, 70, 71]. The authors performed studies on hybrid stars with both constructions. They all concluded that there is no significant difference on the macroscopic properties of the hybrid stars. Due to this fact, in this work we use a Maxwell construction, which is simpler. In this case we impose that the transition occurs when the pressure of the quark matter equals the pressure of the hadronic matter at the same neutron chemical potential:

$$\mu_n^H = \mu_n^Q \quad \text{and} \quad p^H = p^Q, \quad (24)$$

where the neutron chemical potential can be written in terms of the quark ones as:

$$\begin{aligned} \mu_d = \mu_s &= \frac{1}{3}(\mu_n + \mu_e) \\ \mu_u &= \frac{1}{3}(\mu_n - 2\mu_e). \end{aligned} \quad (25)$$

We have seen that in the hadronic phase, when α_v has its value reduced as it moves away from the SU(6) group, the hyperon repulsion increases reducing

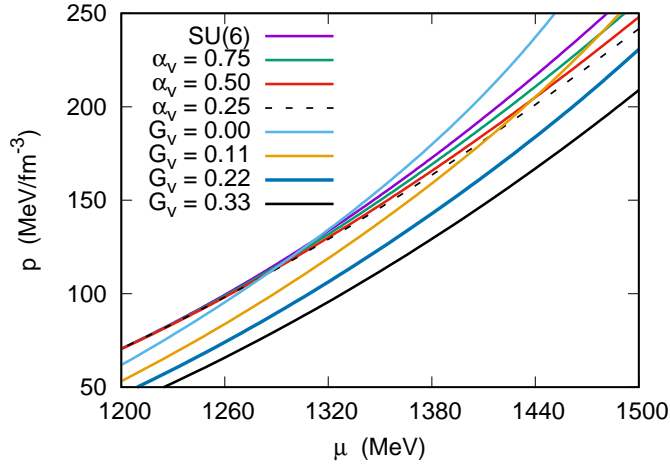


Figure 6: (Color online) Pressure as a function of the neutron chemical potential for several values of α_v in hadronic phase and G_V in quark phase.

the strangeness fraction and therefore producing stiffer EoS and consequently, more massive neutron stars. In the same way, the increase of the G_V value in the quark phase has the same effect: it reduces the strangeness fraction in the core of massive quark stars, stiffening the EoS and producing more massive quark stars. Now we look what is the effect of a stiff/soft EoS in both phases in hybrid stars. To accomplish that, we plot in Fig. 6 the pressure as function of the neutron chemical potential, and seek for the point that satisfies the conditions presented in Eq. (24) for different values of α_v and G_V .

We see that reducing α_v in the hadron phase increases the pressure, so it induces the hadron quark phase transition at early densities when compared with the SU(6) symmetry parametrization. On other hand, the vector channel in the quark phase increases the pressure as well. With the inclusion of the vector channels, the pressure becomes higher in the quark phase than in the hadronic one. For $G_V = 0.22G_s$ the quark phase is already energetically unfavorable, suppressing the phase transition. We see that only for low or zero values of G_V Eq. (24) is not satisfied. Similar behavior has already been noticed in [72]. The phase transition pressure and the critical neutron chemical potential values are

Model	α_v (H)	G_V (Q)	μ^Y (H)	$\mu_n^H = \mu_n^Q$	$p^H = p^Q$	$\epsilon^H(\text{MeV}/fm^3)$	$\epsilon^Q(\text{MeV}/fm^3)$
A0	1.00	$0.00G_s$	1134 MeV	1303 MeV	123 (MeV/fm^3)	642	747
B0	0.75	$0.00G_s$	1142 MeV	1291 MeV	115 (MeV/fm^3)	596	723
C0	0.50	$0.00G_s$	1142 MeV	1285 MeV	111 (MeV/fm^3)	564	710
D0	0.25	$0.00G_s$	1115 MeV	1281 MeV	108 (MeV/fm^3)	542	701
B1	0.75	$0.11G_s$	1142 MeV	1475 MeV	237 (MeV/fm^3)	896	1159
C1	0.50	$0.11G_s$	1142 MeV	1437 MeV	203 (MeV/fm^3)	778	995
D1	0.25	$0.11G_s$	1115 MeV	1418 MeV	187 (MeV/fm^3)	711	929

Table 6: Chemical potential and pressure at phase transition for hadron (H) to quark (Q) with different values of α_v and G_V respectively. We also show the energy density at both phases at the critical neutron chemical potential, and the chemical potential of the hyperon threshold (μ^Y).

presented in Tab. 6.

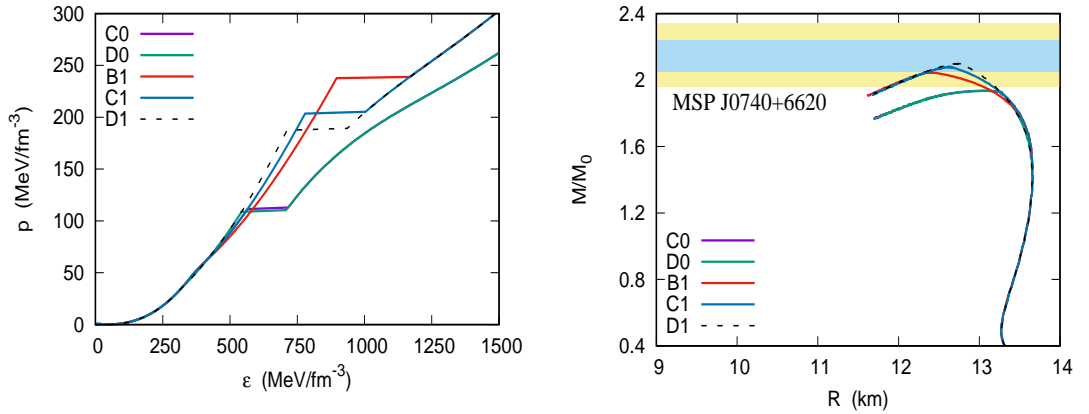


Figure 7: (Color online) EoS and mass-radius relation for models that allow a construction of a hybrid star.

As can be seen, for $G_V = 0.00$, all hadronic EoS allow phase transitions. For $G_V = 0.11G_s$, all but SU(6) allow phase transitions. The lowest critical neutron chemical potential to allow a phase transition is 1281 MeV, at the stiffer hadronic ($\alpha_v = 0.25$) EoS and the softer quark EoS ($G_v = 0.00$). On the other hand, the higher critical neutron chemical potential which still allows a

Model	M/M_\odot	$R(km)$	$n_c (fm^{-3})$	M_{min}/M_\odot
A0	1.92	12.94	0.74	1.91
B0	1.93	13.00	0.73	1.91
C0	1.94	13.07	0.71	1.92
D0	1.94	13.07	0.71	1.92
B1	2.05	12.40	0.78	2.05
C1	2.08	12.64	0.80	2.08
D1	2.10	12.75	0.83	2.09

Table 7: Hybrid star properties indicating that the allowed mass values for a quark core lie within a very narrow band.

phase transition is 1475 MeV, with $\alpha_v = 0.75$ and $G_V = 0.11G_s$.

Another important issue is related to the hyperon puzzle. Can the quark-hadron phase transition suppress the hyperon threshold and solve the hyperon puzzle? As can be seen from Tab. 6 the answer is negative. For all values of α_v , the Λ^0 onset (the first hyperon to appear in all cases) occurs at lower chemical potential (μ^Y) than the critical chemical potential. Our study indicates that the hyperon puzzle is still open even when we are dealing with quark-hadron phase transition.

In order to not saturate the figure, we plot five of the seven possible hybrid star EoS and the mass-radius relation in Fig. 7. The main properties of the hybrid stars are presented in Tab. 7.

As we can see in this work, where all hadronic EoS are derived from the GM1 parametrization [32], and the quark EoS from HK parametrization [55], it is the quark EoS (and not the hadronic one) that plays the more important role in producing different maximum mass values. Although it is model dependent, we believe that qualitatively these features will be maintained with other parameter choices. Fixing $G_V = 0.00$ and varying α_v from 1.00 to 0.25 we produce maximum masses in the range of $1.92M_\odot$ to $1.94M_\odot$. However, when we fix $G_V = 0.11G_s$ the maximum mass now varies from $2.05M_\odot$ to $2.10M_\odot$.

This also indicates that hybrid stars are possible in the context of the massive MSP J0740+6620, only if we consider a vector channel in the NJL model.

Another point to investigate is the M_{min} , which is the minimum mass star that supports a quark core, i.e., stars with masses below M_{min} are purely hadronic. We see that, although the existence of a hybrid star is possible, it is very unlikely, because there is just a narrow mass range that supports a quark core, as already pointed in ref. [18]. Indeed in some cases, the hybrid star branch is lower than $0.01M_{\odot}$, and in other is around $0.02M_{\odot}$. Our results is in agreement with those found in ref. [73], although the authors consider only one hyperon parametrization; also ref. [73] uses constant speed of sound parametrization to determine the phase transition while we use critical neutron chemical potential - $\mu^Q = \mu^H$ at $p^Q = p^H$. The small branch of the hybrid stars is much lower than the experimental uncertainty on the mass of the MSP 0740+6620. Hence, its true nature is still an open subject, although it is unlikely that it is a quark star. Also, hybrid stars always have low central densities when compared with both, quark and hadronic stars. Of course, these results are model dependent and other hadronic and quark models can give different quantitative results.

3.1. The speed of sound and the mass and radius of the quark core

Now we confront our results in the light of a very recent study about the nature of massive stars. In ref. [11], the authors suggest that massive neutron stars have sizable quark core. Moreover, the authors link the size and mass of quark core with the quark matter speed of sound and conclude that the lower the speed of sound of the quark matter, the higher the mass and radius of the quark core. If the square of the speed of sound does not strongly violate the conformal bound - $v_s^2 < 1/3$ - a quark core of mass $0.8M_{\odot}$ and radius around 7 km can be obtained. We start by defining the square of the speed of sound as [13]:

$$v_s^2 = \left| \frac{\partial p}{\partial \epsilon} \right|. \quad (26)$$

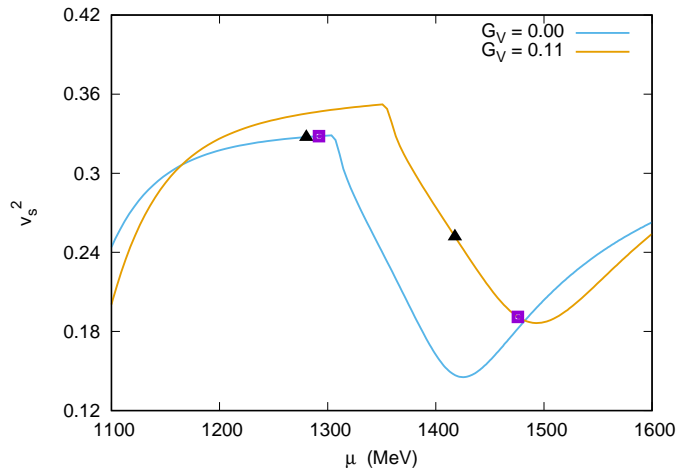


Figure 8: (Color online) Speed of sound for NJL models. The black triangle (purple square) indicates the critical chemical potential for α_V equals to 0.25 (0.75).

Now we plot in Fig. 8 the speed of sound for the NJL model with $G_V = 0.0G_s$ and $G_V = 0.11G_s$ in function of the chemical potential. We also display the critical chemical potential in forms of black triangles and purple squares for the hadronic phase within α_V equals to 0.25 and 0.75 respectively. For $G_V = 0.00G_s$ the speed of sound for all analysed densities is within the conformal bound - $v_s^2 < 1/3$, while for $G_V = 0.11G_s$ there is a small violation around 1300 MeV to 1400 MeV. However the speed of sound at the critical potential is smaller for $G_V = 0.11G_s$. This is due to a peculiar behaviour of the speed of sound in NJL (also pointed in ref. [73]), where at certain density the speed of the sound starts to decrease and then increases again.

To finish our analyses we estimate the mass and size of the quark core in the maximally massive hybrid star of each model presented in Tab. 7. To accomplish that we solve the TOV equations for the quark EoS from the density correspondent to the critical pressure displayed in Tab. 6 up to the density at the maximum mass shown in Tab 7. The results are presented in absolute and relative values in Tab 8.

We see that as in the case of the hybrid branch, it is the quark EoS (over the hadronic one) that produces more massive and larger radii quark cores. For

Model	A0	B0	C0	D0	B1	C1	D1
M_Q/M_\odot	0.052	0.082	0.064	0.079	0.006	0.008	0.014
R_Q (km)	2.61	3.06	2.85	3.05	1.10	1.30	1.57
% M_Q/M_{max}	2.7%	4.2%	3.3%	4.0%	0.3%	0.4%	0.7%
% R_Q/R_{total}	20%	24%	22%	23%	8.9%	10%	12%

Table 8: Masses and radii of the quark core and their proportional contribution for the maximally massive star within different hybrid stars models defined in Tab. 6.

$G_V = 0.00G_s$ the most massive hybrid star can bear a quark core mass around 3% to 4%, while for $G_V = 0.11G_s$ this contribution barely reaches 0.5%. In the same way, for $G_V = 0.00G_s$ the size of the quark core can reach almost 1/4 of the star, while for $G_V = 0.11G_s$ the contribution is only about 10%. In all cases the contribution of the quark phase is more significant in the size than in the mass. Our study corroborates the results of ref. [11], although we found that the quark core plays a much more subtle role than discussed in ref. [11], where its size can reach 60% and the quark core mass reaches 40% of the total mass. Ultimately our results are much closer with those presented in ref. [73], although we use different criteria for the quark-hadron phase transition, as well as different parametrizations.

4. Final Remarks

In this work we broke the hybrid group SU(6) in favor of a more general SU(3) flavor symmetry group to fix the meson-hyperon couplings and employ an additional vector field, the strangeness-hidden ϕ meson, to obtain massive hadronic and hybrid stars. We also investigate the influence of an additional vector channel in the quark phase in the context of NJL models. The main results are summarized below.

- As we move away from the SU(6) group, by reducing α_v we produce stiffer EoS, higher maximum mass and low strangeness fraction. Although the

hyperon onset is well known to soft the EoS, we are still able to produce $2.21M_{\odot}$ hyperonic stars.

- In the quark phase, G_V also increases the pressure, stiffening the EoS. However for realistic values of G_V our maximum mass is quite below the MSP J0740+6620. This possibly indicates that massive pulsars are not quark stars. Although we are able to reproduce a $2.05M_{\odot}$ quark star at the price of using $G_V = G_s$, we believe this vector channel value is artificial and unphysical.
- Stiffening the QHD EoS by reducing α_v , favors the quark-hadron phase transition while stiffening the NJL EoS by increasing G_V makes the phase transition more difficult. Indeed for values of G_V above $0.11G_s$ the quark-hadron phase transition is completely suppressed.
- The quark-hadron phase transition does not solve the hyperon puzzle, as the onset of the Λ^0 hyperons happens for densities lower than those needed for the phase transition to occur for all values of α_V and G_V .
- Within our models, which preserve all the nuclear properties of Tab. 1, as well the quark properties of Tab. 4, it is the quark EoS over the hadronic one that plays a crucial role in the production of more massive hybrid stars.
- According to the models presented in this work, the hybrid star branch is very small, indicating that only stars at the edge of mechanical stability can be hybrid stars. If they exist, hybrid stars are probably very rare in the universe.
- Quark stars can still be present in nature, if the Bodmer-Witten conjecture is true. Low mass hadronic neutron stars can collapse to form a quark star. Massive neutron stars collapse into black holes.
- All our hadronic and hybrid stars present a radius of 13.68 km for the canonical value of $1.4M_{\odot}$. Although it is very close to accepted values

in the literature [43, 46, 45], the possible 11.9 km discussed in ref. [47], adds an additional puzzle either to the EoS or to general relativity. Yet, our results are in agreement with the recent measurements coming from NICER [50, 51].

- We found that the mass of the quark core in a hybrid star is always small, but the radius of the quark core can occupy 1/4 of the star. Qualitatively, our results corroborate the ones coming from ref. [11], but in much more subtle way.
- We can describe even more massive neutron stars if hyperons are not present. However, our results here, as well as others like ref. [6] indicate that hyperons are like Thanos, inevitable.

Acknowledgments This work is dedicated to Liz “Lizuda”. it is a part of the project INCT-FNA Proc. No. 464898/2014-5 and it was partially supported by CNPq (Brazil) under grant 301155.2017-8 (D.P.M.).

References

References

- [1] H. Cromartie et al: Nat. Astr. **4**, 72 (2020)
- [2] J. Antoniadis et al: Science **340**, 1233232 (2013)
- [3] Negreiros et. al., Phys.Lett. B 718 (2013) 1176.
- [4] B. Franzon, V. Dexheimer, S. Schramm Mon. Not. Roy. Astr. Soc. **456**, 2937 (2016)
- [5] R. Gomes, V. Dexheimer, S. Schramm Phys. Rev. D **94** 044018 (2016)
- [6] H. Djapo, B. Schaefer, J. Wambach Phys. Rev. C **81**, 035803 (2010)
- [7] *Avengers: Endgame*, Russo brothers, Marvel Studios, Film (2019)

- [8] E. Witten, Phys. Rev. D **30**, 272 (1984)
- [9] A. R. Bodmer, Phys. Rev. D **4**, 1601 (1971)
- [10] L. McLerran, R. D. Pisarski, Nucl. Phys. A **796**, 83 (2007)
- [11] E. Annala et al., Nat. Phys. **16** 907, (2020)
- [12] B. D. Serot, Rep. Prog. Phys. **55**, 1855 (1992)
- [13] N. K. Glendenning, *Compact Stars*, Springer, New York - Second Edition (2000)
- [14] J. Ellis, J. I. Kapusta, K. A. Olive Nucl. Phys. B **348**, 345 (1991)
- [15] L. L. Lopes, D.P. Menezes, Phys. Rev. C **89**, 025805 (2014)
- [16] R. Cavagnoli, D.P. Menezes, Braz. J. Phys. **35**, 869 (2005)
- [17] S. Weissenborn, D. Chatterjee, and J. Schaffner-Bielich, Phys. Rev. C **85**, 065802 (2012)
- [18] L. Lopes, D. Menezes Eur. Phys. J. **56**, 122 (2020)
- [19] Y. Nambu, G. Jona-Lasinio, Phys. Rev. **122**, 345 (1961)
- [20] L. L. Lopes, D.P. Menezes, Eur. Phys. J. A **52**, 17 (2016)
- [21] J. Sugano et al., Phys. Rev. D **90**, 037901 (2014)
- [22] R. Cavagnoli, D. P. Menezes, C. Providencia, Phys. Rev. C **84**, 065810 (2011).
- [23] L. L. Lopes, D.P. Menezes, Braz. J. Phys. **44**, 744 (2014)
- [24] M. B. Tsang et al, Phys. Rev. C **86**, 015803 (2012)
- [25] M. Oertel et al, Rev. Mod. Phys. **89**, 015007 (2017).
- [26] M. Dutra et al, Phys. Rev. C **90**, 055203 (2014).
- [27] Lattimer & Steiner, Eur. Phys. J. A **50**, 40 (2014)

- [28] H. Pais & C. Providencia, Phys.Rev. C **94**, 015808 (2016)
- [29] V. Dexheimer et al, J.Phys. G **46**, 034002 (2019)
- [30] Providencia et al, Front. Astron. Space Sci., **26** March 2019
- [31] J. Boguta and A.R. Bodmer, Nucl. Phys. A **292**, 413 (1977).
- [32] N. K. Glendenning, S. A. Moszkowski, Phys. Rev. Lett. **67**, 2414 - (1991).
- [33] J. Stone, N. Stone S. Moszkowski, Phys. Rev. C **89**, 044316 - (2014).
- [34] James R. Torres, Francesca Gulminelli and Debora P Menezes, PRC 93, 024306 (2016).
- [35] James R. Torres, Francesca Gulminelli and Debora P. Menezes, PRC 95, 025201 (2017).
- [36] J. J. Swart, Rev. Mod. Phys. **35**, 916 (1963)
- [37] A. Pais, Rev. Mod. Phys. **38**, 215 (1966)
- [38] J. J. Sakurai, Ann. Phys. **11**, 1 (1960)
- [39] W. Greiner, L. Neise, H. Stocker, *Thermodynamics and Statistical Mechanics*, Springer, New York, (1995)
- [40] L. L. Lopes, D.P. Menezes, Braz. J. Phys. **42**, 428 (2012)
- [41] R.C. Tolman, Phys. Rev. 55, 364 (1939); J. R. Oppenheimer, G. M. Volkoff, Phys. Rev. **33**, 374 (1939).
- [42] C. Wynn et al., Mont. Not. Roy. Astron. Soc. **375**, 821 (2007)
- [43] K. Hebeler et al, Phys. Rev. Lett. **105**, 161102 (2010)
- [44] J.M. Lattimer and A.W. Steiner, Astrophys. J. **784**, 123 (2014)
- [45] B. Abbott et al, Phys. Rev. Lett. **121**, 161101 (2018)

- [46] Tuhin Malik, N. Alam, M. Fortin, C. Providência, B. K. Agrawal, T. K. Jha, Bharat Kumar, and S. K. Patra Phys. Rev. C. **98**, 035804 (2018).
- [47] C. Capano et al: Nat. Astr. (2020)
- [48] Clésio E. Mota, Luis C. N. Santos, Guilherme Grams, Franciele M. da Silva and Débora P. Menezes, Phys. Rev. D 100, 024043 (2019)
- [49] L. Lopes and D. P. Menezes, J. Cosm. Astrop. Phys. **05**, 038 (2018)
- [50] T. E. Riley et al., Astrophys. J. Lett. **887**, L21 (2019)
- [51] M. C. Miller et al., Astrophys. J. Lett. **887**, L24 (2019)
- [52] F. Fattoyev, J. Piekarewicz, and C. Horowitz, Phys. Rev. Lett. **120** 172702 (2018)
- [53] D. P. Menezes et al., Phys. Rev. C **89**, 055207 (2014)
- [54] T Hatsuda, T. Kunihiro, Phys. Lett. B **198**, 126 (1987)
- [55] T Hatsuda, T. Kunihiro, Phys. Rep. **247**, 221 (1994)
- [56] M. Kitazawa et al., Prog. Theor. Phys. **108**, 5 (2002)
- [57] T. Klahn, T. Fischer, Astrophys.J. **810**, 134 (2015)
- [58] R. Denke, M. B. Pinto, Phys. Rev. D **88**, 056008 (2013)
- [59] M. Hanauske et al., Phys. Rev. D **64**, 043005 (2001)
- [60] Rhabi et al, J.Phys. G36, 115204 (2009)
- [61] D.P. Menezes et al., J. Cosm. Astrop. Phys. **01**, 024 (2019)
- [62] G. Y. Shao et al., Phys. Rev. D **85**, 114017 (2012)
- [63] G. A. Contrera, A. G. Grunfeld, D. B. Blaschke., Phys. Part. Nucl. Lett. **11**, 4 (2014)
- [64] K. Kashiwa, T. Hell, W. Weise, Phys. Rev. D **84**, 056010 (2011)

- [65] D. P. Menezes, D. B. Melrose, C. Providência, and K. Wu, Phys. Rev. C **73**, 025806 (2006).
- [66] D. P. Menezes and C. Providência, Phys. Rev. C **68**, 035804 (2003).
- [67] H. Beth, G. E. Brown, J. Cooperstein Nucl. Phys. A **462**, 791 (1987)
- [68] B. Serot, H. Uechi Ann. Phys. A **179**, 272 (1987)
- [69] T. Maruyama et al., Phys. Rev. D **76**, 123015 (2007)
- [70] T. Maruyama et al., Phys. Lett. B **659**, 192 (2007)
- [71] M. Paoli, D.P. Menezes, Eur. Phys. J. A **46**, 413 (2010)
- [72] Débora P. Menezes, et al., Phys. Rev. C **89**, 055207 (2014).
- [73] I. Sandoval, et al., Phys. Rev. C **93**, 045812 (2016).